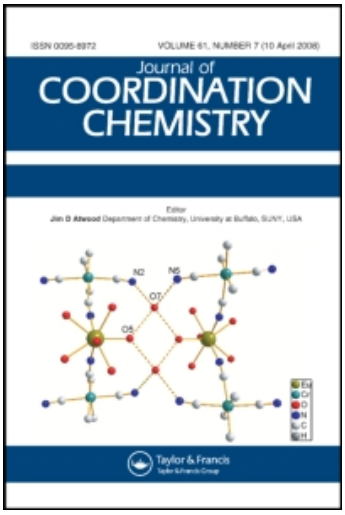

Journal of Coordination Chemistry
Publication details, including instructions for authors and subscription information:
http://www.informaworld.com/smpp/title~content=t713455674

Synthesis, spectroscopy, thermodynamics and structure of [$ZnCl_2$ (η^3-dpktch)] (η^3-dpktch = N,N,O- di-2-pyridyl ketone thiophene-2-carboxylic acid hydrazone)

Mohammed Bakir[a]; Rebecca R. Conry[b]; Orville Green[a]; Willem H. Mulder[a]
[a] Department of Chemistry, The University of the West Indies-Mona Campus, Kingston 7, Jamaica, W. I. [b] Department of Chemistry, Colby College, Waterville, ME 04901-8857, USA

To cite this Article Bakir, Mohammed , Conry, Rebecca R. , Green, Orville and Mulder, Willem H.(2008) 'Synthesis, spectroscopy, thermodynamics and structure of [$ZnCl_2$ (η^3-dpktch)] (η^3-dpktch = N,N,O- di-2-pyridyl ketone thiophene-2-carboxylic acid hydrazone)', Journal of Coordination Chemistry, 61: 19, 3066 — 3079
To link to this Article: DOI: 10.1080/00958970801993672
URL: http://dx.doi.org/10.1080/00958970801993672

Journal of Coordination Chemistry
Vol. 61, No. 19, 10 October 2008, 3066–3079

Taylor & Francis
Taylor & Francis Group

Synthesis, spectroscopy, thermodynamics and structure of [$ZnCl_2$ (η^3-dpktch)] (η^3-dpktch = N,N,O-di-2-pyridyl ketone thiophene-2-carboxylic acid hydrazone)

MOHAMMED BAKIR*†, REBECCA R. CONRY‡, ORVILLE GREEN† and WILLEM H. MULDER†

†Department of Chemistry, The University of the West Indies-Mona Campus, Kingston 7, Jamaica, W. I.
‡Department of Chemistry, Colby College, 5764 Mayflower Hill, Waterville, ME 04901-8857, USA

(*Received 19 June 2007; in final form 21 September 2007*)

When dpktch was reacted with $ZnCl_2$ in refluxing acetonitrile in air [$ZnCl_2$(η^3-dpktch)] was isolated in good yield. Infrared spectra suggest weaker binding of dpktch in [$ZnCl_2$(η^3-dpktch)] than in [$CdCl_2$(η^3-dpktch)]. ^{1}H-NMR studies in non-aqueous media show that [$ZnCl_2$(η^3-dpktch)] is sensitive to changes in its environment and exchanges its amide proton. Electronic absorption spectral measurements confirmed the sensitivity of [$ZnCl_2$(η^3-dpktch)] to changes in its surroundings and show inter-conversion between two intra-ligand-charge-transfer transitions (ILCT) at 330 ± 2 nm and 404 ± 2 associated with [$ZnCl_2$(η^3-dpktch)] and its conjugate base. Thermo-optical measurements in non-aqueous dmf and dmso show facile inter-conversion between [$ZnCl_2$(η^3-dpktch)] and its conjugate base, respectively. Also, it is shown that protonation of dmf by [$ZnCl_2$(η^3-dpktch)] is exothermic (standard enthalpy of protonation $\Delta H^\theta = -40.7 \pm 1.8$ kJ mol^{-1}), but endothermic for dmso ($\Delta H^\theta = +8.3 \pm 1.5$ kJ mol^{-1}). Chemical stimuli in concentrations as low as 5.0×10^{-7} M can be detected and determined using [$ZnCl_2$(η^3-dpktch)] in non-aqueous media. X-ray crystallographic studies on a monoclinic, $P2_1/n$ single crystal of [$ZnCl_2$(η^3-dpktch)] confirmed the N,N,O-coordination of dpktch and revealed interdigitated units of [$ZnCl_2$(η^3-dpktch)] connected via a web of hydrogen bonds.

Keywords: Zinc, di-2-pyridyl ketone thiophene-2-carboxylic hydrazone; X-ray; Optosensing; Thermodynamics; Synthesis

1. Introduction

Di-2-pyridyl ketone derivatives that include oxime and hydrazones (see scheme 1) and their metal compounds continue to attract attention because of their interesting physico-chemical properties and their applications in many important areas such as medicine, photography, nonlinear optics, liquid crystals, molecular sensing and catalysis [1–11]. We reported on the synthesis, characterization, structures and optosensing behavior of a variety of di-2-pyridyl ketone derivatives and in recent reports described the optosensing

*Corresponding author. Email: mohammed.bakir@uwimona.edu.jm

ISSN 0095-8972 print/ISSN 1029-0389 online © 2008 Taylor & Francis
DOI: 10.1080/00958970801993672

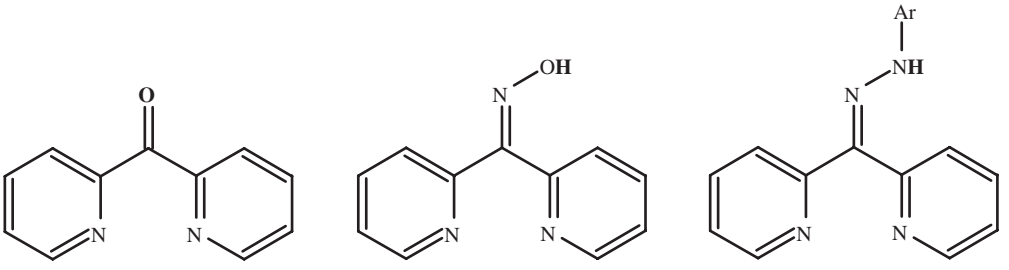

dpk **dpkoxime** **dpkhydrazone**

Scheme 1. Di-2-pyridyl ketone derivatives.

behavior of di-2-pyridyl ketone thiophene-2-carboxylic acid hydrazone (dpktch) [12–25]. Optical measurements on dpktch in non-aqueous solvents show facile inter-conversion between two molecular conformations that are sensitive to changes in their surroundings [14]. Optosensing measurements show that group-12 metal dichlorides in concentrations as low as 1×10^{-5} M can be detected and determined using dpktch in non-aqueous media. ^{1}H-NMR studies in non-aqueous media confirmed the sensitivity of dpktch to changes in its surroundings and showed two isomers/conformations at low temperature; when the temperature increased one isomer predominates. Although the optosensing behavior of dpktch in aqueous media and the synthesis of two of its tin complexes and their bioactivities were reported over ten years ago, literature on the coordination chemistry of dpktch is scarce [26, 27]. In a recent report we described the synthesis, characterization, and X-ray structural analysis of the first cadmium compound of dpktch, and in this report we describe the isolation, physico-chemical properties and structure of [$ZnCl_2$(η^3-dpktch)] and compare the results with those reported for [$CdCl_2$(η^3-dpktch)] [15].

2. Experimental

2.1. *Reagents and Reaction Procedures*

Solvents were reagent grade and thoroughly deoxygenated prior to use. The compound dpktch was prepared following a standard procedure employed for the synthesis of dpkhydrazones [14]. All other reagents were obtained from commercial sources and used without further purification.

2.2. *Preparation of [$ZnCl_2$(η^3-dpktch)]*

A mixture of $ZnCl_2$ (200 mg, 1.47 mmol), dpktch (500 mg, 1.62 mmol) and acetonitrile (60 mL) was refluxed in air for 1h. The resulting reaction mixture was reduced in volume to 30 mL and allowed to cool to room temperature. A yellow precipitate was filtered off, washed with hexane, diethyl ether and dried; yield 500 mg (76%). Anal. Calcd. for $C_{16}H_{12}Cl_2N_4OSZn$ (%): C, 44.84; H, 2.82; N, 13.07%). Found: C, 44.80; H, 2.73; N, 12.94. Infrared data (KBr disk, cm^{-1}): ν (N–H) $\sim$ 3450 broad, ν (C–H) $\sim$ 3068, ν(C=O) 1610, ν(C=N and C=C of pyridine) 1598–1550. UV–Vis {λ/nm, (ε/$cm^{-1}M^{-1}$)}: in DMF or DMSO 330 [3,500 (α) and 18,600 (β)] and 400 [24,500 (α) and 0 (β)]. ^{1}H NMR (δ ppm)

in dmso-d_6: 13.73 (0.40 H), 9.00 (1 H), 8.72 (1 H), 8.11 (2 H), 8.02 (4 H), 7.82 (1 H), 7.70 (1H), 7.65 (1H) and 7.30 (1 H).

2.3. *Optical sensing studies*

A stock solution of [$ZnCl_2(\eta^3$-N,N,O-dpktch)] in a polar, non-aqueous solvent, and stock solutions of a stimulus ($NaBH_4$, $NaBF_4$) in a polar non-aqueous solvent were prepared separately. Optical changes (electronic absorption spectral changes) were measured on solutions prepared by mixing appropriate volumes of [$ZnCl_2(\eta^3$-N,N,O-dpktch)] and stimulus solutions to prepare the desired solutions (see figure captions for details). All measurements were made at room temperature.

2.4. *Molecular orbital calculations*

Monte Carlo semi-empirical molecular orbital calculation using default parameters on the lowest triplet was performed using the Hyperchem molecular modeling program [28].

2.5. *Physical measurements*

Electronic absorption spectra were recorded on a HP-8452A spectrophotometer. Baseline corrections on blank solvents were recorded prior to measurements. A Lauda-Brinkmann RM6 circulating bath was used for temperature control. ^{1}H NMR spectra were recorded on a Bruker ACE 500-MHz Fourier-transform spectrometer and referenced to the residual protons in the incompletely deuteriated solvent. Infrared spectra were recorded as KBr pellets on a Perkin-Elmer Spectrum 1000 FT-IR Spectrometer.

2.6. *X-ray crystallography*

Crystals of [$ZnCl_2(\eta^3$-dpktch)] were obtained from a dmso solution of [$ZnCl_2(\eta^3$-dpktch)] that was allowed to stand for several days. A single crystal was selected and mounted on a glass fiber with epoxy cement. A Bruker SMART CCD area-detector diffractometer with Mo-Kα radiation and a graphite monochromator was used for data collection and the SHELXTL software package version 5.1 was used for structure solution [29–31]. Cell parameters and other crystallographic information are given in table 1 along with additional details concerning data collection. All non-hydrogen atoms were refined with anisotropic thermal parameters.

2.7. *Analytical procedures*

Elemental microanalyses were performed by MEDAC Ltd., Department of Chemistry, Brunel University, Uxbridge–United Kingdom.

3. Results and discussion

The reaction between $ZnCl_2$ and dpktch in refluxing acetonitrile in air gave [$ZnCl_2(\eta^3$-dpktch)] (see scheme 2) in good yield. This reaction is similar to that reported for the

Table 1. Crystal data and structure refinement for [$ZnCl_2(\eta^3$–dpktch)].

Empirical formula	$C_{16}H_{12}Cl_2N_4OSZn$
Formula weight	444.63
Temperature (K)	297(2)
Wavelength (Å)	0.71073
Crystal system, space group	Monoclinic, $P2_1/n$
Unit cell dimensions (Å, °)	
a	9.1926(5)
b	13.4224(7)
c	14.4161(8)
α	90
β	95.7560(10)
γ	90
Volume (Å^3)	1769.79(17)
Z, Calculated density (Mg m^{-3})	4, 1.669
Absorption coefficient (mm^{-1})	1.820
F(000)	896
Crystal size(mm^3)	$0.32 \times 0.28 \times 0.10$
θTheta; range for data collection (°)	2.08–28.22°
Range of h, k, l	−12/12, −17/17, −19/19
Reflections collected/unique	16443/4312 [$R_{(int)} = 0.0588$]
Completeness to $\theta = 28.22$	98.7%
Refinement method	Full-matrix least-squares on F^2
Data/restraints/parameters	4312/0/230
Goodness-of-fit on F^2	1.013
Final R indices [$I > 2\sigma(I)$][a,b]	$R_1 = 0.0336$, $wR_2 = 0.0795$
R indices (all data)	$R_1 = 0.0471$, $wR_2 = 0.0822$
Largest diff. peak and hole (e Å^{-3})	0.452 and −0.299

[a] $R_1 = R_1 = \sum \|F_o| - |F_c\| / \sum |F_o|$.
[b] $wR_2 = \{\sum [w(F_o^2 - F_c^2)^2] / \sum w(F_o^2)^2]\}^{1/2}$ where $w = 1/[\sigma^2(F_o^2) + (0.0462P)^2 + 0.0000\text{P}]$ and $\text{P} = (F_o^2 + 2F_c^2)/3$.

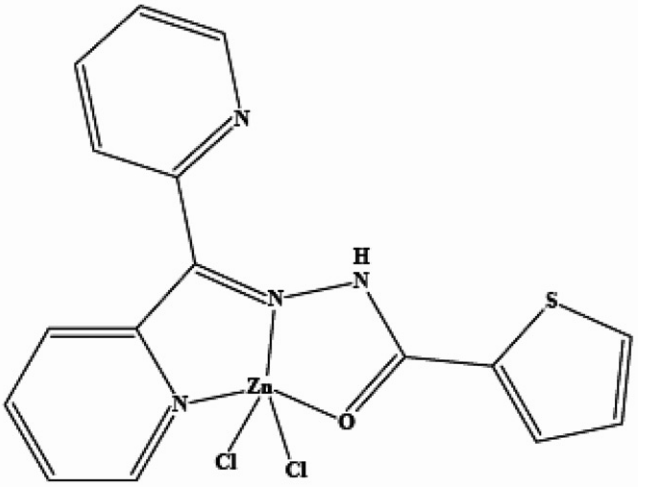

Scheme 2. [$ZnCl_2(\eta^3$–dpktch)].

synthesis of $[CdCl_2(\eta^3\text{-dpktch})]$ [15]. The identity of the isolated compound as $[ZnCl_2(\eta^3\text{-dpktch})]$ was based on the results of its elemental analysis and a number of spectroscopic measurements, as well as an X-ray structural analysis done on a crystal $[ZnCl_2(\eta^3\text{-dpktch})]$ grown from dmso. The IR spectrum of $[ZnCl_2(\eta^3\text{-dpktch})]$ shows a band at 1610 cm^{-1} due to the amide I $\tilde{\nu}$(C=O) vibration. The amide I C=O vibration appeared at 1603 and 1655 in $[CdCl_2(\eta^3\text{-dpktch})]$ and dpktch, respectively [14,15]. The $\tilde{\nu}$(C=O) peak for $[ZnCl_2(\eta^3\text{-dpktch})]$ appeared at higher wavenumbers compared to $[CdCl_2(\eta^3\text{-dpktch})]$ suggesting weaker binding of $ZnCl_2$ than $CdCl_2$ to dpktch. The combined $\tilde{\nu}$(C=C) and $\tilde{\nu}$(C=N) vibrations of the pyridyl groups and the N–H out-of-plane wagging vibration appeared in the same region as was observed in $[CdCl_2(\eta^3\text{-dpktch})]$. The ^{1}H-NMR spectra of $[ZnCl_2(\eta^3\text{-dpktch})]$ measured in d_6-dmso and d_7-dmf along with the spectrum of dpktch in dmso are shown in figure 1. These spectra show that $[ZnCl_2(\eta^3\text{-dpktch})]$ is sensitive at solvent variations. The amide proton of coordinated dpktch is observed as a broad singlet at 13.37 and 13.68 ppm in d_6-dmso and d_7-dmf, respectively, at 298 K. The integrated relative intensities for these peaks are 0.4 and 0.3 instead of the expected 1.0 and hint at proton exchange between $[ZnCl_2(\eta^3\text{-dpktch})]$ and aprotic solvent. In the free ligand, the amide proton appeared at 13.40 ppm and for $[CdCl_2(\eta^3\text{-dpktch})]$ two signals appeared in the amide region at 15.24 and 13.43 ppm in d_6-dmso at 298 K. Subtle variations in the chemical shifts of the aromatic protons of $[ZnCl_2(\eta^3\text{-dpktch})]$ *versus* dpktch and in different solvents at 298 K

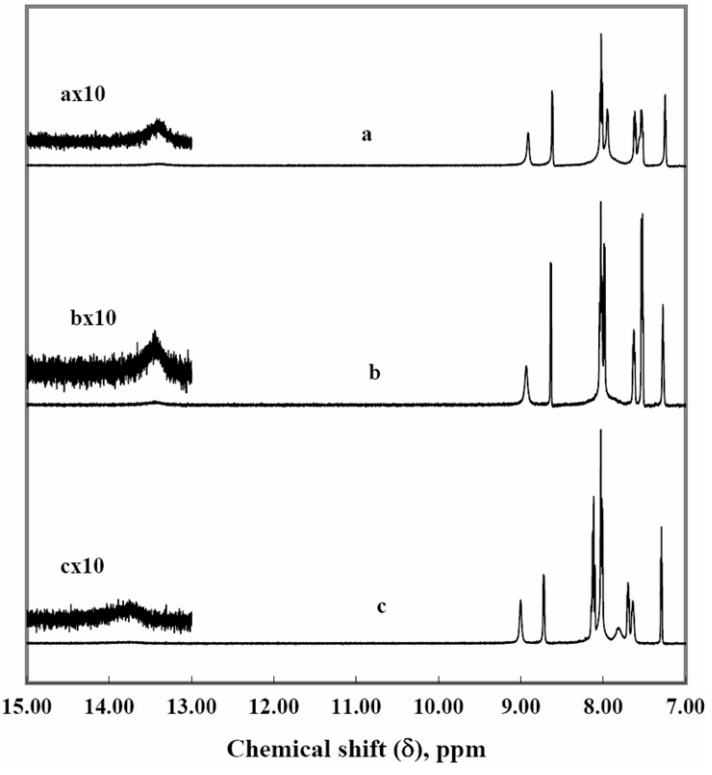

Figure 1. ^{1}H-NMR spectra of $[ZnCl_2(\eta^3\text{–dpktch})]$ measured in d_6-dmso (a) and d_7-dmf (c) and dpktch (b) in d_6-dmso.

were noted, consistent with binding of $ZnCl_2$ to dpktch and the sensitivity of [$ZnCl_2$(η^3-dpktch)] to solvents. Variable temperature ^{1}H-NMR studies for [$ZnCl_2$(η^3-dpktch)] show the disappearance of the amide proton and changes in the chemical shifts of the aromatic protons. These results confirm the solvent-complex interaction and exchange of the amide proton with its surroundings, and indicate a sensitivity of these systems (metal compound and surrounding solvent molecules) to slight changes in their surroundings.

The electronic absorption spectra of [$ZnCl_2$(η^3-dpktch)] in different solvents are shown in figure 2 and point to a strong solvent-complex interaction. The low and high energy electronic transitions between 500 – 300 nm in dmf and dmso appeared at similar energy as those reported for the free ligand and [$CdCl_2$(η^3-dpktch)] and suggest a keto-enol-tautomerization or an acid-base inter-conversion as shown in scheme 3. These transitions are due to $\pi \rightarrow \pi^*$ of the pyridine ring followed by pyridine $\rightarrow$ thiophene-2-carboxylic acid charge-transfer. Semi-empirical molecular orbital Monte Carlo calculational results (see figure 3) are consistent with the assigned electronic transitions and gave a HOMO $\rightarrow$ LUMO energy gap of 3.13 eV, corresponding to absorption at a wavelength of 396 nm. The variation in intensity of the electronic transitions may be due to the extent of solvent–solute interactions. In dmf, a highly intense absorption band appeared at 405 nm and in dmso, two peaks appeared at 406 and 330 nm. The intensity of the low energy to high energy electronic transitions of [$ZnCl_2$(η^3-dpktch)] in

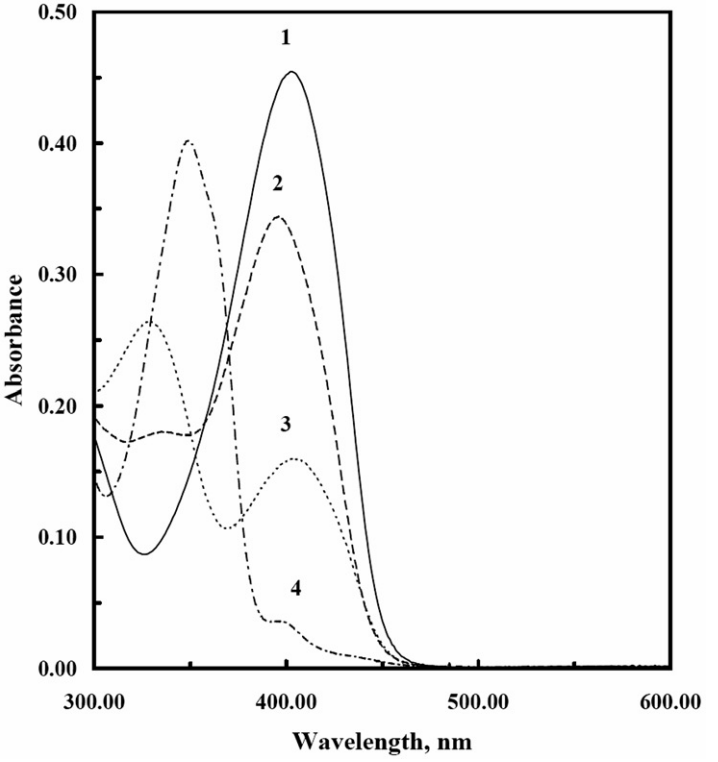

Figure 2. Electronic absorption spectra of [$ZnCl_2$(η^3–dpktch)] 2.0×10^{-5} M measured in dmf (1), CH_3CN (2), dmso (3) and CH_2Cl_2 (4).

dmso are concentration dependent. As the concentration of [$ZnCl_2(\eta^3$-dpktch)] decreases, the ratio of the absorbance at low energy to the absorbance at high energy increases. These results are in accord with the NMR results that show exchange of the amide proton of [$ZnCl_2(\eta^3$-dpktch)] in aprotic solvents and confirm the acid-base inter-conversion or keto-enol tautomerization and assign the high energy electronic transition to [$ZnCl_2(\eta^3$-dpktch)] and the low energy electronic transition to its conjugate base (see scheme 3).

The electronic absorption spectra of [$ZnCl_2(\eta^3$-dpktch)] are highly sensitive to the presence of various chemical stimuli. The electronic absorption spectra of [$ZnCl_2(\eta^3$-dpktch)] in dmso recorded at increasing amounts of $NaBH_4$ are shown in figure 4 and these results demonstrate that $NaBH_4$ in concentrations as low as 5.0×10^{-7} M can be detected using [$ZnCl_2(\eta^3$-dpktch)] in dmso. In the presence of excess $NaBH_4$ in dmso, extinction coefficients can be determined at the wavelengths corresponding to the peak maxima, where presumably either a protonated, α, form predominantly absorbs (330 nm), or the deprotonated, β form (405 nm; see table 2). The difference between the assignment of the alpha peak and result of the ab initio study must be due to a

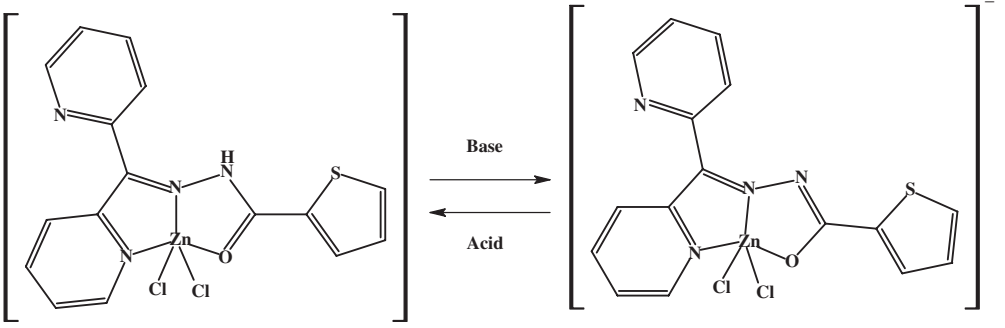

Scheme 3. Keto-enol or acid-base inter-conversion of [$ZnCl_2(\eta^3$–dpktch)].

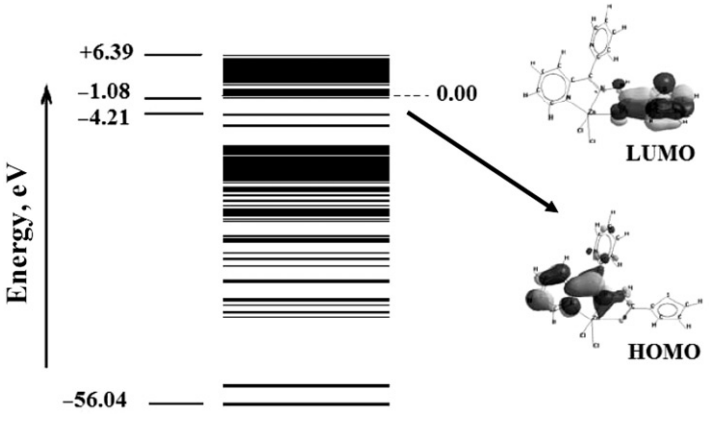

Figure 3. Semi-empirical molecular orbital energy diagram for [$ZnCl_2(\eta^3$–dpktch)].

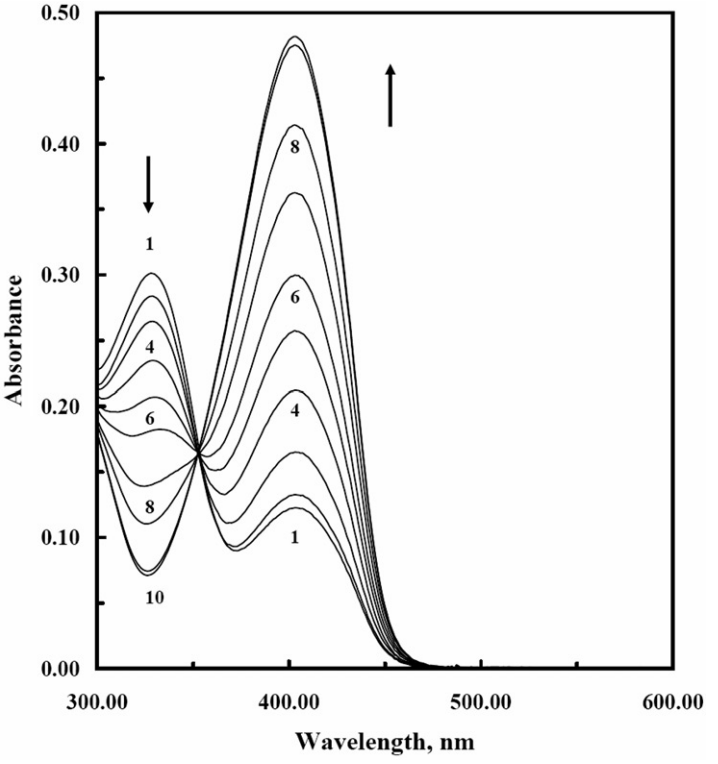

Figure 4. The electronic absorption spectra of [$ZnCl_2(\eta^3$–dpktch)] 2×10^{-5} M in dmso in the presence of 0.00 (1), 5×10^{-7} (2), 1.5×10^{-6} (3), 3.5×10^{-6} (4), 5.5×10^{-6} (5), 7.5×10^{-6} (6), 1.00×10^{-5} (7), 2.00×10^{-5} (8), 3.00×10^{-5} (9), 4.00×10^{-5} M $NaBH_4$ (10).

Table 2. Extinction coefficients of [$ZnCl_2(\eta^3$–dpktch)] in dmso and dmf (± 300, in $M^{-1}cm^{-1}$).

Solvent	$\varepsilon^{\beta}_{300}$	$\varepsilon^{\alpha}_{300}$	$\varepsilon^{\beta}_{400}$	$\varepsilon^{\alpha}_{400}$
dmso	3,500	18,600	24,500	0
dmf	3,500	20,000	24,000	0

solvatochromic (blue) shift. In dmf, the extinction coefficients were calculated by the same method, in the presence and absence of excess $NaBH_4$.

Variable temperature electronic absorption spectral studies on a dmf solution of [$ZnCl_2(\eta^3$-dpktch)] showed a decrease in the intensity of the low-energy electronic transition with increasing temperature, while that of the high-energy electronic transition increased. The reverse was observed when the temperature was lowered or when dmso was used in place of dmf. These results established reversible interconversion between the low and high energy electronic transitions of [$ZnCl_2(\eta^3$-dpktch)] and indicate that dmf and dmso have different proton affinities toward [$ZnCl_2(\eta^3$-dpktch)]. Spectra obtained at varying temperatures reveal that dmf has a stronger affinity for the (amide) proton than dmso, as shown by the high intensity of the low energy electronic transition in dmf and the presence of a significant peak maximum at

high energy in dmso. This hints at exothermic and endothermic proton transfer in dmf and dmso, respectively. A plot of $R\ln K$ (K is the equilibrium constant for the reaction $\alpha + S \leftrightarrow \beta + SH^+$, where S is an aprotic solvent and α denotes α-[$ZnCl_2(\eta^3$-dpktch)] and β denotes β-[$ZnCl_2(\eta^3$-dpktch)]), *versus* $10^3/T$ gave straight lines (see figure 5) with gradients of $+40.7 \pm 1.8$ and -8.3 ± 1.5 and intercepts of -199.8 ± 5.5 and -77.5 ± 4.9 in dmf and dmso, respectively, giving thermodynamic parameters shown in table 3.[1] The low values for the thermodynamic parameters confirm the sensitivity of [$ZnCl_2(\eta^3$-dpktch)] to its surroundings and potential use as a molecular sensor.

Values of ΔG^θ indicate that it is more difficult for the complex to protonate dmso than dmf, as observed earlier. The reaction enthalpies are consistent with the anticipated endothermicity of solvent protonation in dmso, compared to exothermicity in dmf. The negative reaction entropies reflect increased ordering of the polar solvent due to the charged products. Values for the pK's were obtained both from the temperature study and the dilution experiments, and were found to be consistent.

The solid state structure of [$ZnCl_2(\eta^3$-dpktch)] was determined using single crystal X-ray crystallography. A view of the molecular structure of [$ZnCl_2(\eta^3$-dpktch)] is shown in figure 6. The zinc ion exhibits pseudo-trigonal bipyramidal coordination resulting from the binding of two chlorides, two nitrogens and one oxygen. The observed coordination mode is similar to that of [$CdCl_2(\eta^3$-dpktch)] and other related compounds of the type [$MCl_2(\eta^3$–L)] where L = is a tridentate N,O,N ligand and M=Zn or Cd [15,32]. The bond distances and angles of [$MCl_2(\eta^3$-dpktch)], where M=Zn or Cd are shown in table 4. The variations in bond distances are normal and consistent with change in the covalent radii of the metals. The O1MN3 and N1MN3 bite angles of [$ZnCl_2(\eta^3$-dpktch)] are larger than those of [$CdCl_2(\eta^3$-dpktch)], which suggests a less strained metallocyclic ring in the case of [$ZnCl_2(\eta^3$-dpktch)], and stronger binding of dpktch to $CdCl_2$ compared to $ZnCl_2$. Indices of trigonality (τ) of 0.41 and

[1] For the following proton-exchange equilibrium: $\alpha + S \rightleftarrows \beta + SH^+$ the total absorbance at wavelength λ equals

$$A_\lambda = \varepsilon_\lambda^\alpha[\alpha] + \varepsilon_\lambda^\beta[\beta] = \varepsilon_\lambda^\beta c + \left(\varepsilon_\lambda^\alpha - \varepsilon_\lambda^\beta\right)[\alpha],$$

where $c = [\alpha] + [\beta]$ is the total concentration. Thus,

$$[\alpha] = \left(A_\lambda - \varepsilon_\lambda^\beta c\right)/\left(\varepsilon_\lambda^\alpha - \varepsilon_\lambda^\beta\right)$$

and

$$[\beta] = \left(\varepsilon_\lambda^\alpha c - A_\lambda\right)/\left(\varepsilon_\lambda^\alpha - \varepsilon_\lambda^\beta\right),$$

so that the equilibrium constant $K = [\beta]^2/[a]$ at temperature T equals

$$K(T) = \frac{\left(\varepsilon_\lambda^\alpha c - A_\lambda(T)\right)^2}{\left(A_\lambda(T) - \varepsilon_\lambda^\beta c\right)\left(\varepsilon_\lambda^\alpha - \varepsilon_\lambda^\beta\right)}$$

(independent of λ; ε's are temperature independent because of the observed isosbestic points). The thermodynamic parameters characterizing the solvent protonation reaction are then obtained from a plot of $R\ln K$ vs. $1/T$ according to

$$-\frac{\Delta G^\theta}{T} = R\ln K = \Delta S^\theta - \frac{\Delta H^\theta}{T}$$

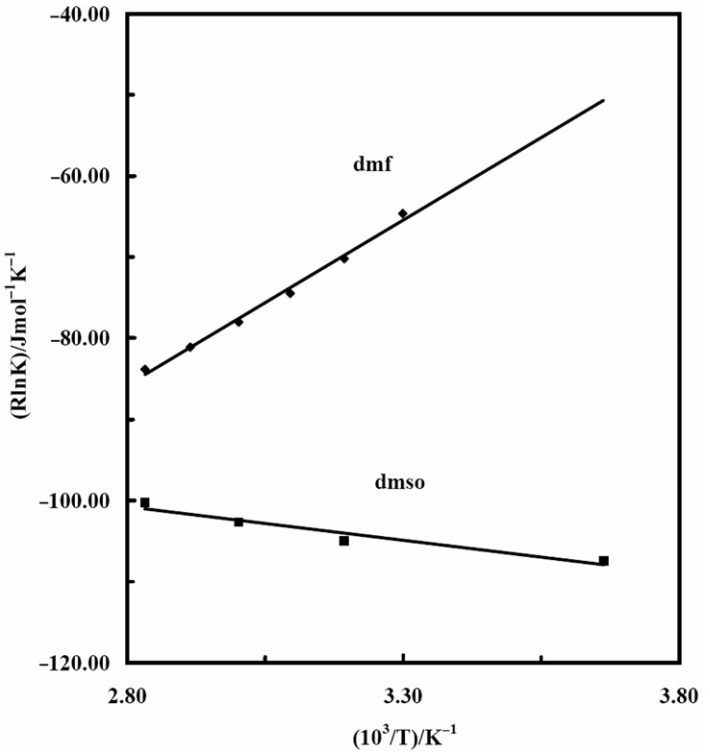

Figure 5. A plot of $R\ln K$ *vs.* $10^3/T$ of 2.0×10^{-5} *M* [$ZnCl_2(\eta^3$–dpktch)] in dmf and dmso.

Table 3. Thermodynamic parameters for the protonation of dmf and dmso by [$ZnCl_2(\eta^3$–dpktch)].

Solvent	ΔH^θ/kJ mol^{-1}	ΔS^θ/J K^{-1} mol^{-1}	ΔG^θ/kJ mol^{-1} (25°C)	pK (25°C)
dmf	-40.7 ± 1.8	-199.8 ± 5.5	$+18.9 \pm 2.4$	3.3 ± 0.2
dmso	$+8.3 \pm 1.5$	-77.5 ± 4.9	$+31.4 \pm 2.1$	5.5 ± 0.2

0.30 were calculated for [$ZnCl_2(\eta^3$-dpktch)] and [$CdCl_2(\eta^3$-dpktch)], respectively, and show that [$ZnCl_2(\eta^3$-dpktch)] more strongly favors trigonal-bipyramidal geometry compared to [$CdCl_2(\eta^3$-dpktch)] [15, 33].[2]

The packing of [$ZnCl_2(\eta^3$-dpktch)] is shown in figure 7 and reveals interdigitated units of [$ZnCl_2(\eta^3$-dpktch)] connected via a network of hydrogen bonds. Views of the non-covalent hydrogen bonds are shown in figure 8. The chlorides link various stacks by forming bifurcated hydrogen bonds with adjacent molecules. Chlorine atom 1 forms

[2] For a five-coordinate system similar to that shown in figure 8, the trigonality index $\tau = (\beta - \alpha)/60$ where $\beta = \angle$N1–Zn1–O1, $\alpha = \angle$N3–Zn1–Cl1. Thus $\tau = 0$ for a perfect tetragonal geometry and $\tau = 1$ for a perfect trigonal-bipyramidal geometry.

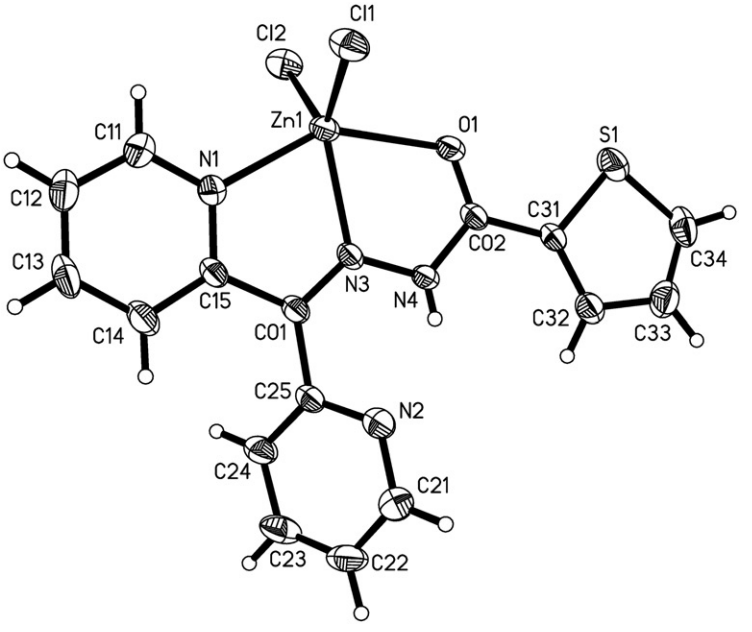

Figure 6. A view of the molecular structure of [$ZnCl_2(\eta^3$–dpktch)]. The thermal ellipsoids are drawn at the 30% probability level.

Table 4. Bond lengths [Å] and angles [°] for [$MCl_2(\eta^3$–dpktch)] where M=Zn or Cd.

	[$ZnCl_2$(**η³-dpktch**)]	[$CdCl_2$(**η³-dpktch**)]
M–N(3)	2.1465(17)	2.368(3)
M–N(1)	2.1594(17)	2.361(3)
M–Cl(1)	2.2331(7)	2.4299(12)
M–O(1)	2.2355(14)	2.385(3)
M–Cl(2)	2.2410(6)	2.4079(12)
N(1)–C(11)	1.332(3)	1.341(6)
N(1)–C(15)	1.339(3)	1.345(5)
C(01)–N(3)	1.292(2)	1.293(4)
N(4)–C (01)	1.356(2)	1.357(5)
C(02)–O(1)	1.220(2)	1.235(4)
N(3)–M–N(1)	72.56(6)	67.19(11)
N(3)–M–O (1)	71.52(6)	66.94(9)
N(1)–M–Cl(2)	100.10(5)	102.50(9)
N(3)–M–Cl(2)	126.38(5)	130.69(9)
Cl(2)–M–O(1)	98.69(5)	101.82(8)
N(1)–M–Cl(1)	101.64(5)	103.73(10)
N(3)–M–Cl(1)	119.21(5)	115.50(9)
O(1)–M–Cl(1)	98.16(5)	101.64(8)
Cl(2)–M–Cl(1)	114.32(2)	113.78(4)
C–N(4)–N(3)	115.50(18)	117.0(3)
C(02)–O(1)–M	116.11(12)	118.2(2)

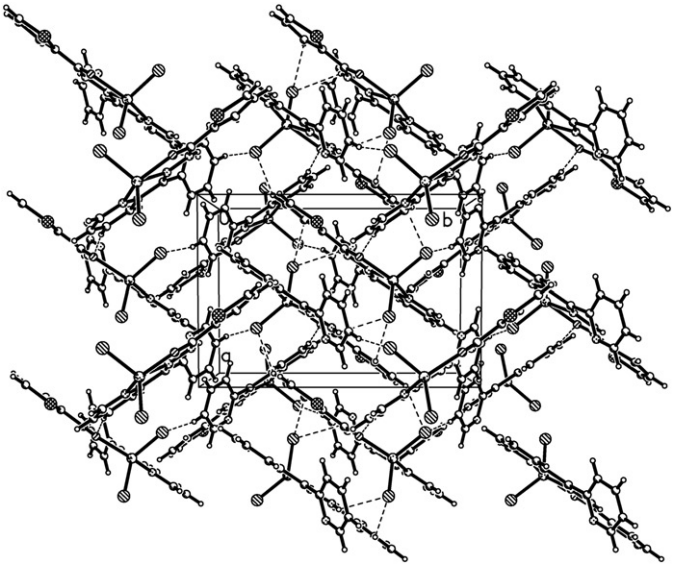

Figure 7. Packing of molecules of [$ZnCl_2$(η^3–dpktch)]. Non-covalent hydrogen bonds are represented by dashed lines.

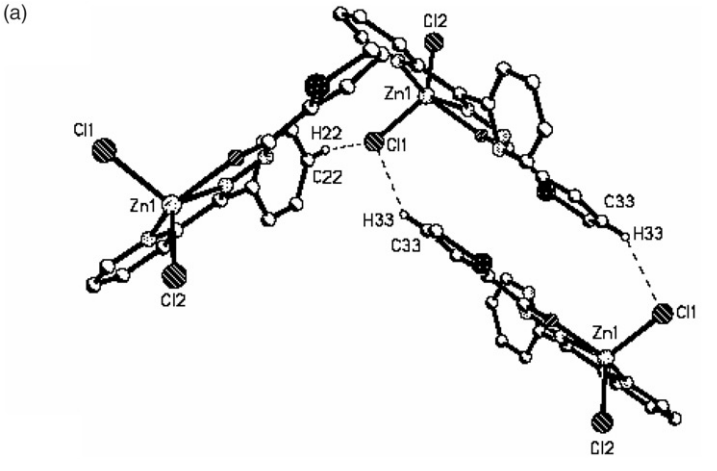

Figure 8. Views of the non-covalent hydrogen bonds in the packed structure of [$ZnCl_2$(η^3–dpktch)].

non-classic hydrogen bonds of the type C–H···Cl with two different adjacent [$ZnCl_2$(η^3-dpktch)] molecules (see figure 8a) while chloride 2 forms a classic hydrogen bond and a non-classic hydrogen bond of the types N–H···Cl and C–H···Cl, respectively, with one adjacent [$ZnCl_2$(η^3-dpktch)] (see figure 8b). The oxygen of coordinated dpktch forms a non-classic hydrogen bond of the type C–H···O with an adjacent coordinated pyridine ring (see figure 8c). The bond distances and angles of the non-covalent bonds (see table 5) are of the same order as those reported for other compounds containing such bonds [34].

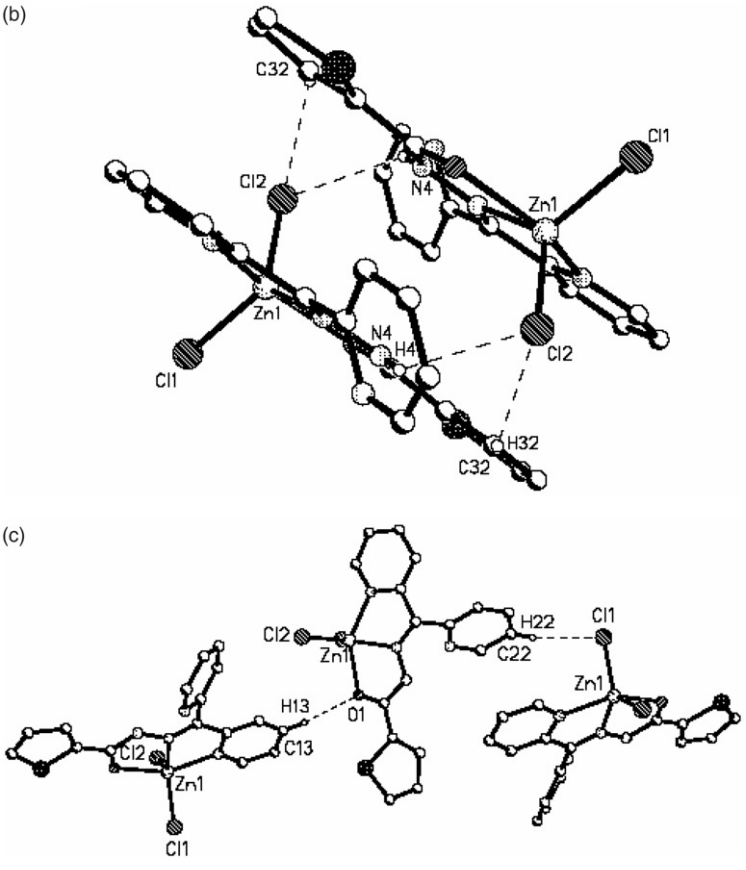

Figure 8. Continued.

Table 5. Hydrogen bonds for [$ZnCl_2(\eta^3$–dpktch)].

D–H···A	d(D–H)	d(H···A)	d(D···A)	<(DHA)
N(4)–H(4) ···N(2)	0.72(2)	2.27(2)	2.793(3)	131(2)
N(4)–H(4)···Cl(2)^{i}	0.72(2)	2.90(2)	3.421(3)	132(2)
C(13)–H(13)···O(1)^{ii}	0.93	2.45	3.372(3)	173.5
C(34)–H(34)···N(2)^{iii}	0.93	3.20	3.444(3)	97.6
C(22)–H(22)···Cl(1)^{iv}	0.93	2.76	3.678(3)	167
C(33)–H(33)···Cl(1)^{v}	0.93	3.20	3.444(3)	97.6
C(32)–H(32)···Cl(2)^{i}	0.93	2.89	3.551(3)	129.4

Symmetry transformations used to generate equivalent atoms: (i) $-x, -y, -z$, (ii) $x-1/2, -y+1/2, z+1/2$, (iii) $-x+1, -y, -z$, (iv) $-x+1/2, y-1/2, -z+1/2$, and (v) $-x+1, -y, -z$

4. Conclusion

Isolation of [$ZnCl_2(\eta^3$-dpktch)] marks the first time a zinc compound of dpktch has been isolated. Spectroscopic measurements elucidated the coordination of dpktch and the sensitivity of the compound to slight changes in its surroundings. Electrochemical measurements revealed sequential electronic transition and

decomposition of [$ZnCl_2$(η^3-dpktch)]. X-ray structural analysis confirmed the identity of the isolated compound, divulged distorted trigonal bipyramidal coordination about zinc, and showed a network of hydrogen bonds connecting all the molecules in the extended structure.

Acknowledgments

We wish to thank Ms. Toni Johnson for NMR measurements.

References

[1] D.R. Richardson, P.C. Sharpe, D.B. Lovejoy, D. Senaratne, D.S. Kalinowski, M. Islam, P.V. Bernhardt. *J. Med. Chem.*, **49**, 6510 (2006).
[2] Z. Chen, F. Liang, S. Zhou, C. Xia, R. Hu. *J. Mol. Struct.*, **827**, 20 (2007).
[3] A. Escuer, G. Aromi, Guillem. *Eur. J. Inorg. Chem.*, **23**, 4721 (2006).
[4] B.F. Abrahams, T.A. Hudson, R. Robson. *Chemistry – A Eur. J.*, **12**, 7095 (2006).
[5] C.J. Milios, A. Prescimone, J. Sanchez-Benitez, S. Parsons, M. Murrie, E.K. Brechin. *Inorg. Chem.*, **45**, 7053 (2006).
[6] C. Papatriantafyllopoulou, C.G. Efthymiou, C.P. Raptopoulou, R. Vicente, E. Manessi-Zoupa, V. Psycharis, A. Escuer, S.P. Perlepes. *J. Mol. Struct.*, **829**, 176 (2007).
[7] Y. Li, S. Xiang, T. Sheng, J. Zhang, S. Hu, R. Fu, X. Huang, X. Wu. *Inorg. Chem.*, **45**, 6577 (2006).
[8] E.B. Seena, B.N.B. Raj, M.R.P. Kurup, E. Suresh. *J. Chem. Cryst.*, **36**, 189 (2006).
[9] M.C. Suen, J.C. Wang. *Inorg. Chem. Commun.*, **9**, 478 (2006).
[10] B. Asc, G. Alpdogan, S. Sungur. *Anal. Lett.*, **39**, 997 (2006).
[11] P. Antonio, K. Iha, K. Suarez-Iha. *Talanta*, **64**, 484 (2004).
[12] M. Bakir, J.A.M. McKenzie. *J. Electroanal. Chem.*, **425**, 61 (1997).
[13] M. Bakir, I. Hassan, O. Green. *J. Coord. Chem.*, **59**, 1953 (2006).
[14] M. Bakir, C. Gyles. *J. Mol. Struct.*, **833**, 161 (2007).
[15] M. Bakir, M.A.W. Lawrence, M. Singh-Wilmot. *J. Coord. Chem.*, **60**, 2385 (2007).
[16] M. Bakir. *J. Electroanal. Chem.*, **466**, 60 (1999).
[17] M. Bakir, K. Abdur-Rashid. *Trans. Metal Chem.*, **24**, 384 (1999).
[18] M. Bakir, K. Abdur-Rashid, W.H. Mulder. *Talanta*, **51**, 735 (2000).
[19] M. Bakir, C. Gyles. *Talanta*, **56**, 1117 (2002).
[20] M. Bakir, C. Gyles. *J. Mol. Struct.*, **753**, 35 (2005).
[21] M. Bakir, O. Green, C. Gyles. *Inorg. Chim. Acta*, **358**, 1835 (2005).
[22] M. Bakir, O. Brown, T. Johnson. *J. Mol. Struct.*, **691**, 265 (2004).
[23] M. Bakir, K. Abdur-Rashid, C. Gyles. *Spectrochim. Acta Part A*, **59**, 2123 (2003).
[24] M. Bakir. *Eur. J. Inorg. Chem.*, **2**, 481 (2002).
[25] M. Bakir. *Inorg. Chim. Acta*, **332**, 1 (2002).
[26] A.Z. Abuzuhri, M.S. Elshahawi, M.M. Kamal, M. Alnuri, M. Hannoun. *Anal. Lett.*, **27**, 1907 (1994).
[27] M. Carcelli, C. Pelizzi, G. Pelizzi, P. Mazza, F. Zani. *J. Organomet. Chem.*, **55**, 488 (1995).
[28] Hyper Chem 7.5 Professional Edition, Hyper Cube, Inc., 1115 NW 4th Street, Gainesville, Florida 32601, USA.
[29] Bruker-SMART (2001). Software Version 5.625. Brucker AXS, Inc., Madison, Wisconsin, U.S.A.
[30] Bruker-SHELXTL, Software Version 5.1. Brucker AXS, Inc., Madison, Wisconsin, USA, 1997.
[31] G.M. Sheldrick, *SHELX*97 and *SHELXL*97, University of Göttingen, Germany (1997).
[32] C.E. Kyriakidis, P.C. Christidis, P.J. Rentzeperis, I.A. Tossidis. *Z. Kristallogr.*, **193**, 261 (1990).
[33] A.W. Addison, T.N. Rao, J. Reedijk, J.v. Rijn, G.C. Verschoor. *J. Chem. Soc.-Dalton Trans.*, 1349 (1984).
[34] M. Bakir, I. Hassan, T. Johnson, O. Brown, O. Green, C. Gyles, M.D. Coley. *J. Mol. Struct.*, **688**, 213 (2004).